JOURNAL OF MATERIALS SCIENCE 25 (1990) 1463–1467

A geometrical model on the angular effect in Auger electron spectroscopy

JIN YU
Department of Materials Science and Engineering, Korea Advanced Institute of Science and Technology, PO Box 131, Chongryang, Seoul, Korea

In Auger electron spectroscopy of temper-embrittled specimens, Auger signals emanating from fractured grain boundaries vary from grain to grain, and the anisotropy in grain-boundary segregation due to the varying grain-boundary structure is primarily responsible for it. Here, another anisotropy, due to the varying angle between the grain boundaries and the incident electron beam, is considered by extending the geometrical model of Matsudaira and Onchi to the cylindrical mirror analyser geometry. Results suggest that the angular effect may explain a substantial amount of the spread in measured Auger peak height ratios.

1. Introduction

Over the past twenty years, Auger electron spectroscopy (AES) has become an essential tool in the study of grain-boundary and surface-segregation phenomena. In performing AES for the study of impurity-induced embrittlement in polycrystalline low-alloy steels, it has always been observed that the Auger signals vary from grain boundary to grain boundary, and that the Auger peak height ratios (PHR) from a polycrystalline sample form a broad spectrum of distribution as typically shown by Powell and Woodruff [1] in Cu–Bi alloys. This can mainly be ascribed to the anisotropy of segregation in which grain boundaries of varying structures have varying heats of segregation (ΔH). It is known that the low-angle or coincidence boundaries have high ΔH, while high-angle grain boundaries have low ΔH [2]. Therefore, distribution characteristics of various types of boundaries primarily determine the Auger signal distributions emanating from the polycrystalline samples.

In addition to this intrinsic anisotropy of segregation arising from varying grain-boundary structures, there is an angular effect which is extrinsically determined by the angle between the primary beam and the specimen surface. The angular effect is mainly associated with the variations in the detected volume as the specimen is tilted from the normal incidence [3–7]. However, as the orientation of the specimen varies, the emission angle also changes and the outcoming Auger signal varies as a function of both incidence and emission angle. The problem is more complicated when there is a segregated adsorbate layer on the substrate.

An example which qualitatively demonstrates the nature of the angular effect is shown in Figs 1a–f which correspond to the fracture surface of a temper-embrittled $2\frac{1}{4}$Cr–1Mo steel [8], and Auger maps of P_{120}, Fe_{703}, Mo_{186}, C_{273} and Cr_{529}, respectively. Note that the variation in Auger signals is more or less consistent among the elements, and the angular effect is expected to diminish substantially when PHR is used. However, measured PHR values which are shown in Fig. 1g tend to be higher for the inclined boundaries (cf. grains 7, 8, 14, 15 with 2 and 5 in Figs 1a and g). If variations in Auger PHR coming from the angular effect are not negligible, they may be important in quantitative AES of polycrystals where fracture paths along grain boundaries easily deflect $\pm$ 60° along its path. It is the purpose of the present work to provide very simple estimates of the variation of Auger PHR with incidence angle in a cylindrical mirror analyser (CMA) system.

2. The model

The model is purely geometrical and is based on that of Matsudaira and Onchi [3]. The assumptions used by Matsudaira and Onchi [3] are mostly employed here, and thus omitted. According to the model, the number of Auger electrons, dI, which reach the detector from layer, dz, in a pure metal is given by

$$dI \sim (1 + r) P_i P_A \left[I_p \frac{\cos\beta}{S} \exp\left(- \frac{z}{\lambda_{p_r} \cos\beta} \right) \right] \times \left(\frac{S}{\cos\beta} \right) \left(\frac{dz}{\cos\beta} \right) \frac{d\Omega}{4\pi} \left[\exp\left(- \frac{z}{\lambda_A \cos\theta} \right) \right] \quad (1)$$

where, r is a correction term for the Auger emission out of the back-scattered incident beam, P_i is the probability of ionization of the inner shell necessary to produce the Auger peak of interest, P_A is the emission probability of the Auger electron of interest against X-ray photon or other Auger transitions, I_p is the intensity of the primary beam, β is the angle of incidence, S is the beam area, z is the shortest distance from the surface, λ_{pr} is the mean free path of the primary electrons, $d\Omega$ is the acceptance solid angle of the detector, and λ_A is the mean free path of the Auger electron. The geometry of the model considered by Matsudaira and Onchi [3] is shown in Fig. 2. Then, the

0022–2461/90 $03.00 + .12

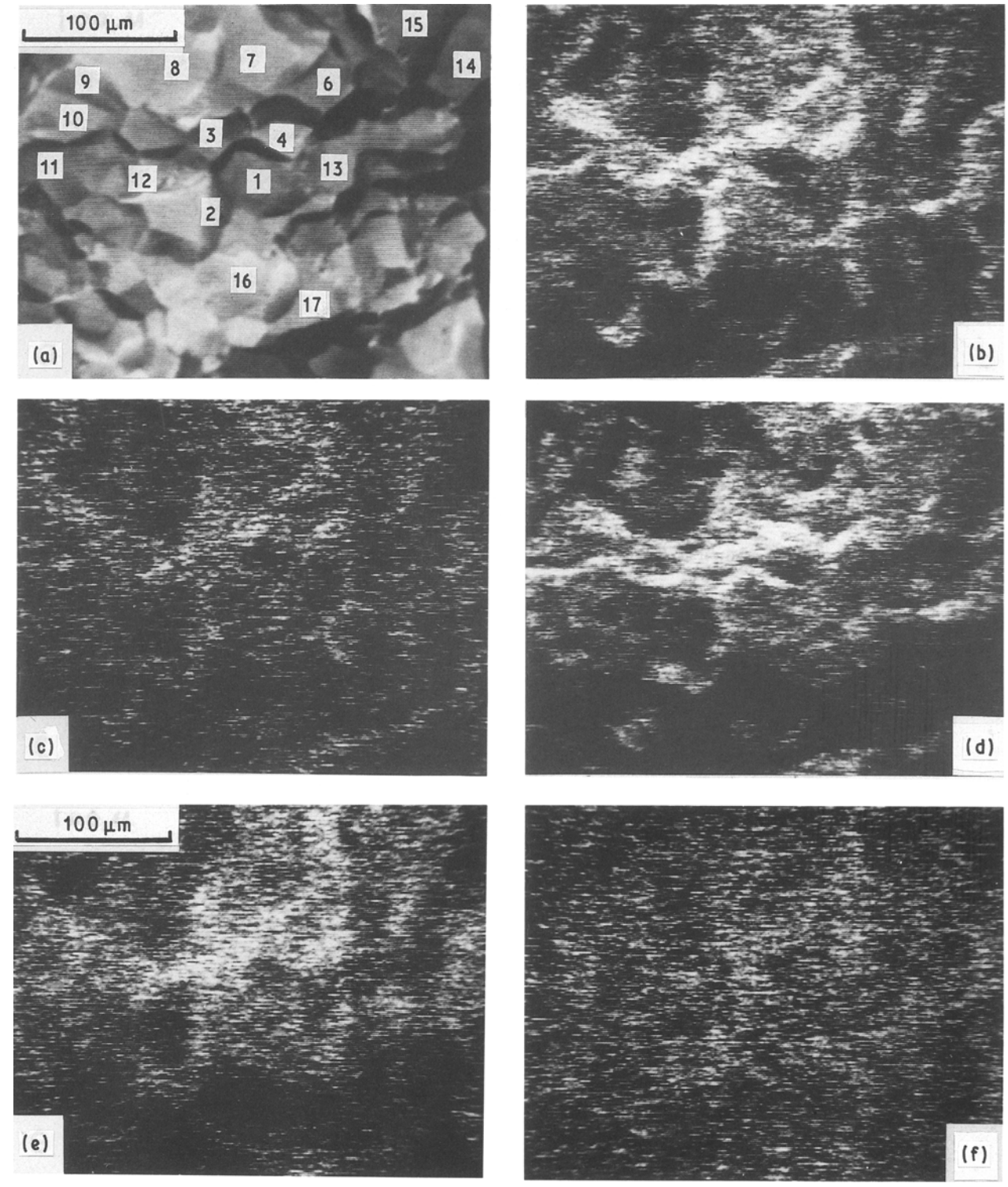

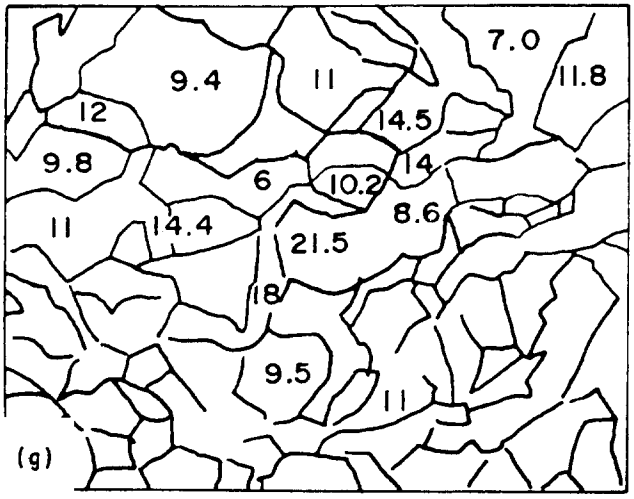

Figure 1 (a) Scanning electron micrograph from the fracture surface of a temper-embrittled $2\frac{1}{4}$ Cr–1Mo steel, and the elemental Auger maps of (b) P_{120}, (c) Mo_{186}, (d) Fe_{703}, (e) C_{273}, and (f) Cr_{5229} peaks. Measured P_{120} and Fe_{703} PHRs (%) from various grain boundaries are marked in (g).

total Auger current is given by integrating dI over the specimen thickness.

By a simple extension of the approach to a binary alloy with a segregated layer, it can be easily seen that the ratio of the number of Auger electrons entering the detector out of the solute atom A with respect to those out of the solvent atom B is given by

$$\frac{I_A}{I_B} = \frac{\int_0^{l'} X_A^s dI_A + \int_{l'}^{\infty} X_A^b \, dI_A}{\int_0^{l'} X_B^s dI_A + \int_{l'}^{\infty} X_B^b \, dI_B} \qquad (2)$$

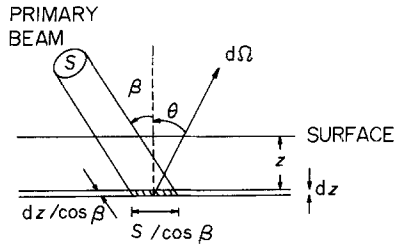

Figure 2 Geometry of the model for angular dependence used by Matsudaira and Onchi [3].

where, l is the thickness of the segregated layer and superscripts s and b denote the surface and the bulk phase, respectively. For example, X_A^s denotes the concentration of the solute in the surface layer. The first term in the numerator denotes the number of Auger electrons of the element A from the surface layer and the second term corresponds to those of the same element from the substrate layer, and vice versa.

When the coaxial CMA is used, the situation is not so simple. For the normal incidence of the primary beam, the tilt angle is zero and the emission angle to CMA slit is 42.3°. As the specimen is tilted away from the normal incidence, attenuation of the primary beam and the emitted Auger electron beam both vary as a function of the tilt angle, which is schematically shown in Fig. 3. To reach the dz layer, the primary beam travels $dz/\cos\beta$, but the distance Auger electrons travel in the metal toward the CMA slit (z') varies with the rotation angle ϕ as shown in Fig. 4a. From the geometry shown in Fig. 4b, it can be easily shown that

$$z' = \frac{z}{\cos\theta(\cos\beta - \tan\theta\cos\phi\sin\beta)} \quad (3)$$

Because z and z' are both positive, Equation 1 for the coaxial CMA can be written as

$$dI = (1+r)\left[I_p\frac{\cos\beta}{S}\exp\left(-\frac{z}{\lambda_p\cos\beta}\right)\right] \times\left(\frac{S}{\cos\beta}\right)\left(\frac{dz}{\cos\beta}\right)\frac{1}{2\pi}\int_0^{2\pi} \times\exp\left(-\frac{z}{\lambda_A\cos\theta\,|\cos\beta - \tan\theta\cos\phi\sin\beta|}\right)d\phi \quad (4)$$

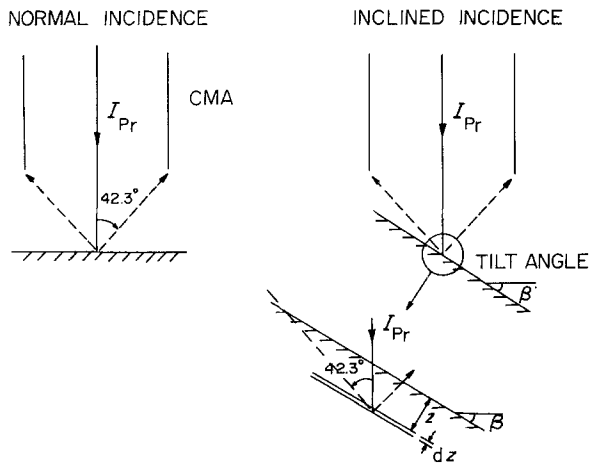

Figure 3 Geometry of the present model for the normal and inclined incidences when CMA is used.

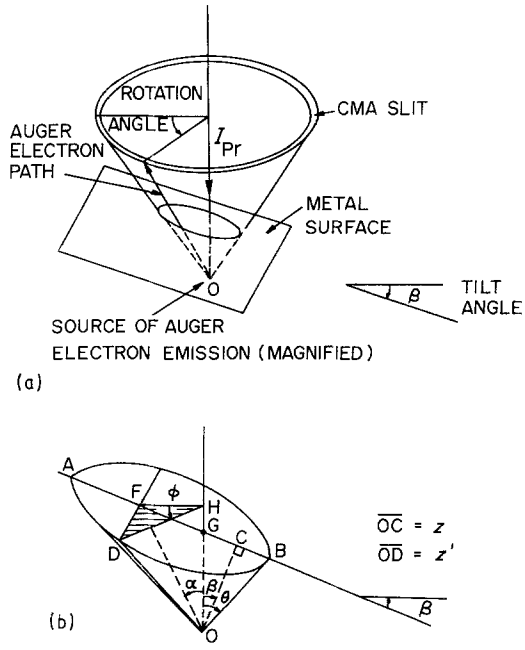

Figure 4 Schematic diagrams showing (a) the travel paths of Auger electrons from the inside of the specimen to the CMA slit, and (b) the travel path in the specimen.

Here, an additional factor of $\frac{1}{2}\pi$ is introduced due to integration over angle ϕ. However, Equation 4 does not apply when the tilt angle is greater than $(\pi/2)-\theta$ because of the shadowing of the CMA slit by the sample, as shown in Fig. 5. In such a case, the lower limit of integration should be changed to

$$\phi_0 = \cos^{-1}\left\{\frac{\tan[(\pi/2)-\beta]}{\tan\theta}\right\}$$

and the upper limit to $2\pi-\phi_0$ in Equation 4. Also, in applying Equations 2 and 4 to the study of the surface with a segregated surface with a segregated layer, it is usually asssumed that back-scattering factors are the same for the primary and Auger electrons, and for the substrate and adsorbant, just for the sake of convenience.

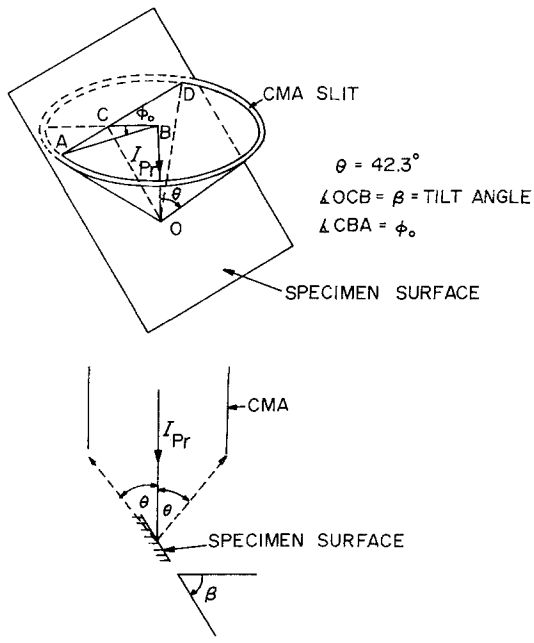

Figure 5 Shadowing of the CMA slit by the sample for tilt angles greater than 47.7°.

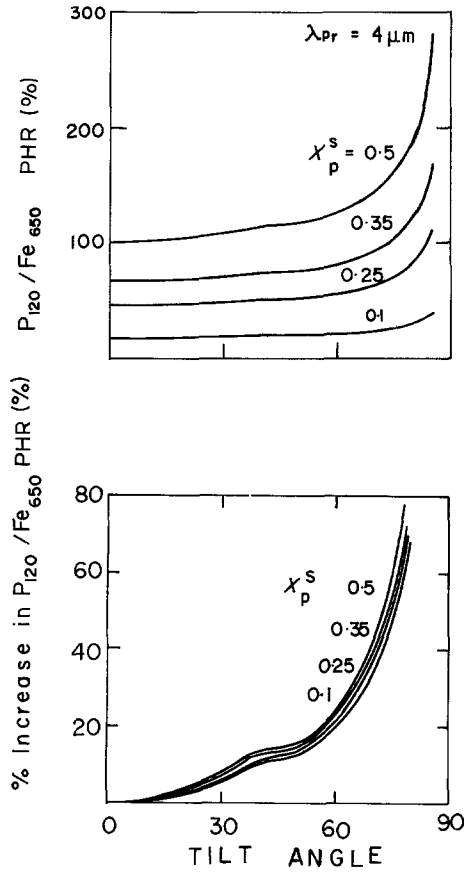

Figure 6 Calculated P_{120} and Fe_{650} PHRs as functions of the tilt angle at several surface concentrations of phosphorus.

3. Results and discussion

The model is used to calculate the Auger PHR of an Fe–P alloy using the material parameters shown in Table I. By assuming that $X_{Fe}^{b} = 1$ and that $P_i P_A$ is the same for iron and phosphorus, PHRs of P_{120} compared to Fe_{650} are calculated for various phosphorus compositions (X_p^s) in the surface layer, and the results are presented in Fig. 6a and b. Note that the calculated P_{120}/Fe_{650} PHR for $X_p^s = 0.5$ is close to 1, which is consistent with the experimental result by Erhart and Grabke [10] who studied [1 0 0] Fe single crystal with a phosphorus layer of c (2 × 2) structure on the surface. The angular effect, which can be manifested as the increase of the relative PHR with the tilt angle, shows that the angular effect increases with the tilt angle, but the effect is relatively insensitive to the adsorbate concentration for $X_p^s > 0.1$. For $X_p^s = 0.5$ and $B = 60°$, the PHR increases only 24%, as compared to the 40% predicted from the Matsudaira and Onchi [3] model. Thus, it can be seen that the angular effect is attenuated when the CMA geometry is taken into account, and that there is a discontinuity in the rate of increase of relative PHR with the tilt angle at $\beta = 42.3°$, which is obviously caused by the shadowing effect.

TABLE I Material parameters

λ_{Pr}	4 nm
λ_P	0.4 nm
λ_{Fe}	1.2 nm
l_{Fe}	0.248 nm
θ	42.3°

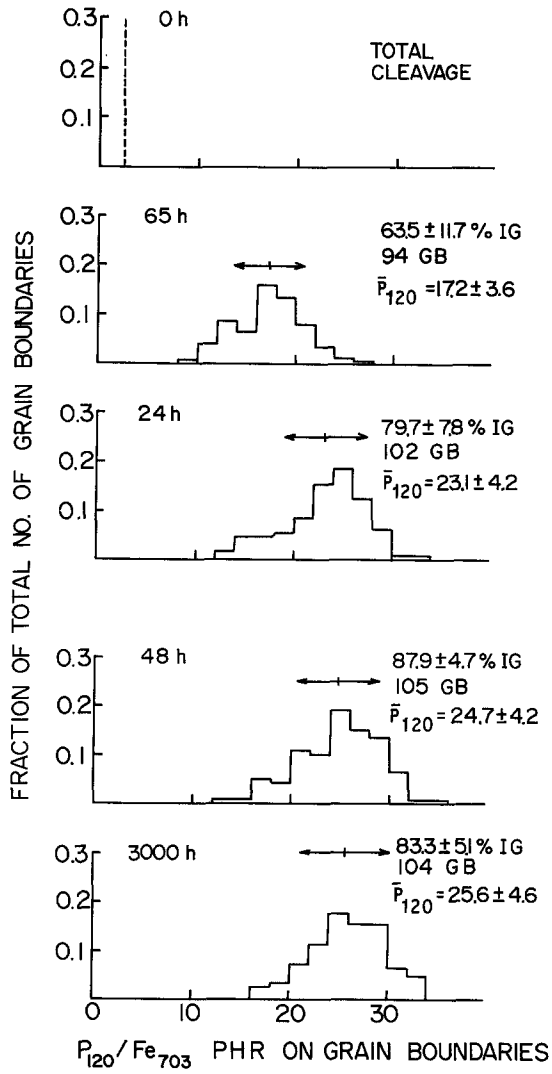

Figure 7 Histograms of P_{120} and Fe_{703} PHRs for an embrittled $2\frac{1}{4}$ Cr–1Mo–0.6Si–0.7Mn–0.2C steel at varying ageing times at 793 K, where $\bar{P}_{120}$ is the average P_{120}.

Other experimental data which may be compared with the predictions of the present model are shown in Fig. 7. Using a temper-embrittled $2\frac{1}{4}$ Cr–1 Mo steel doped with 0.04 P, 0.7 Mn and 0.6Si, AES was conducted for 50 to 100 grain boundaries at various ageing times, and the results show that the histograms of intergranular phosphorus concentration usually have standard deviations corresponding to ~20% of their mean values. Assuming that most of the grain boundaries lie within ± 60° from the macroscopic crack plane, predictions of the present model suggest that the angular effect may account for a substantial part of the spread in the observed histograms. For the quenched and tempered condition where the intergranular fracture percentage is 62%, only high-angle grain boundaries with high heats of segregation can be thought to be separated, and variations in the grain boundary structure among fractured grain boundaries may not be significant.

The present model is purely geometrical and ignores any complications arising from the directionality of bonding or back-scattering of electrons, and more elaborate experiments need to be done.

3. Conclusions

Previous geometrical models on the angular effect

have been improved to include the CMA geometry. It suggests that a substantial portion of the spread in measured Auger PHRs emanating from fractured polycrystalline sample can be ascribed to this effect.

Acknowledgements

This work was conducted while the author was affiliated with the University of Pennsylvania, USA.

References

1. B. D. POWELL and D. P. WOODRUFF, *Phil. Mag.* **34** (1976) 169.
2. T. WATANBE, *J. de Physique, Colloque* **4** (1985) C4–555.
3. T. MATSUDAIRA and M. ONCHI, *Surf. Sci.* **72** (1978) 7118.
4. S. J. WHITE, D. P. WOODRUFF and L. McDONELL, *ibid.* **72** (1978) 77.
5. K. HORN, A. M. BRADSHAW and W. JACOBI, *ibid.* **72** (1978) 719.
6. R. HERTLEIN, R. WEISSMANN and K. MULLER, *ibid.* **77** (1978) 118.
7. L. A. HARRIS, *ibid.* **15** (1969) 77.
8. JIN YU and C. J. McMAHON Jr, *Met. Trans.* **11** (1980) 291.
9. M. P. SEAH, in "Practical Surface Analysis", edited by D. Briggs and M. P. Seah (Wiley, 1983) p. 247.
10. H. ERHART and H. J. GARBKE, *Met. Sci.* **15** (1981) 401.

Received 23 November 1988
and accepted 3 May 1989